Hindawi
International Journal of Chemical Engineering
Volume 2024, Article ID 8434050, 15 pages
https://doi.org/10.1155/2024/8434050

Research Article

Hydrothermally Produced Activated Carbon Impregnated with ZnO for the Adsorptive Removal of Toxic Pharmaceutical Contaminants from Aqueous Solution

Kilaru Harsha Vardhan,[1,2] **Hrishitha Sree**,[1,2] **P. Senthil Kumar**,[3] **and B. Senthil Rathi**[1,2]

[1]*Department of Chemical Engineering, Sri Sivasubramaniya Nadar College of Engineering, Kalavakkam 603110, Tamil Nadu, India*
[2]*Centre of Excellence in Water Research (CEWAR), Sri Sivasubramaniya Nadar College of Engineering, Kalavakkam 603110, Tamil Nadu, India*
[3]*Centre for Pollution Control and Environmental Engineering, School of Engineering and Technology, Pondicherry University, Kalapet, Puducherry 605014, India*

Correspondence should be addressed to Kilaru Harsha Vardhan; kilaruh@ssn.edu.in and P. Senthil Kumar; senthilkumarp@pondiuni.ac.in

Received 7 February 2024; Revised 7 March 2024; Accepted 29 April 2024; Published 15 May 2024

Academic Editor: Li Qingchao

This research explores the adsorption (AD) of diclofenac sodium (DS) onto a Hydrothermally produced activated carbon impregnated with ZnO (HTC-AC/ZnO) surface, considering various factors such as initial concentration (IC), adsorbent dose, contact time, and pH. The characterization of HTC-AC/ZnO was performed using X-ray diffractometer (XRD), scanning electron microscope (SEM), Fourier-transform infrared spectroscopy (FTIR), and nitrogen physisorption spectroscopy (BET). Tests were conducted with different adsorbent doses (0.5–4 g/L) at 303 K and various initial diclofenac concentrations (ranging from 50 mg/L to 250 mg/L) to observe their effects. Additionally, pH values were altered from 2 to 12 to study their influence on AD. Kinetic studies, thermodynamic studies, and AD isotherm models were examined. The Temkin isotherm model (TIM) was found to be the most accurate for DS-AD on HTC-AC/ZnO. For DS-AD on HTC-AC/ZnO, pseudo-first-order models (PFOM), intraparticle diffusion model (IPDM), and pseudo-second-order models (PSOM) were applied, with a correlation coefficient of 0.945, indicating a good fit for PFOM. The kinetics suggested rapid adsorption. Notably, the HTC-AC/ZnO composite exhibited consistent AD characteristics across four consecutive cycles, with a removal efficiency exceeding 99.38%. This suggests that HTC-AC/ZnO is an appropriate and economically viable adsorbent for the elimination of DS from water-based solutions. The investigation provides compelling evidence that HTC-AC/ZnO is a viable adsorbent for the effective elimination of DS from water sources.

1. Introduction

In even the most developed nations, emerging contaminants (ECs) represent uncontrolled substances that pose risks to human well-being and ecology [1]. La Farré et al. [2] define these contaminants as substances that encompass chemical pesticides, flame retardants, plasticizers, food additives, medications, personal care products, wood preservatives, laundry detergents, surfactants, disinfectants, and hormonal substances, both organic and artificial. Among these substances, pharmaceutical contaminants (PCs) are the most frequently encountered heterocyclic aromatic products [3]. These PC substances are typically found in small quantities (ranging from parts per billion to parts per million) in wastewater treatment (WWT) facilities [4]. Primary sources of PC pollutants include wastewater from healthcare facilities, communities, and pharmaceutical companies [5]. Wang et al. [6] highlight the potential for pharmaceutical

contaminant (PC) pollution to disrupt aquatic ecology and pose risks to human health. Consequently, the development of efficient techniques to control their levels in the atmosphere is imperative [7].

One of the most frequently encountered pharmaceutical contaminants is NSAID or nonsteroidal anti-inflammatory drugs. These medications are widely employed in treating conditions such as gout, arthritis, migraines, and other inflammatory disorders by mitigating discomfort and inflammation [8]. Among NSAIDs, DS stands out as the most commonly used one—an analgesic employed in the treatment of joint, muscle, and tendon disorders, primarily reducing pain, swelling, and inflammation [9]. However, DS is not entirely metabolized following ingestion. Due to limitations in current sewage treatment facilities, approximately 15% of its active ingredient remains unremoved, ultimately being expelled into the atmosphere [10]. Consequently, DS has been detected in both ground and drinking waters. Its presence in water systems has deleterious effects: it disrupts the endocrine glands of marine and terrestrial organisms, interferes with the metabolic pathways of microbes in soil and water, and impedes sunlight penetration into the water [11]. Lonappan et al. [12] note that the overuse of DS causes host organisms to become resistant.

Several techniques such as chemical oxidation [13], biodegradation [14], photo-degradation [15], nano-filtration [16], reverse osmosis [17], and anaerobic digestion (AD) [18] are available for the elimination of DS from WW. However, most of these methods come with certain drawbacks, such as energy consumption and the generation of toxic byproducts. Among these, AD stands out as a technique that is user-friendly, cost-effective, swift, efficient, and devoid of harmful byproducts [19, 20]. Alessandretti et al. [21] have extensively documented the use of various adsorbents, including carbon nanotubes, activated carbon (AC) [22], metal-organic frameworks [23], metals, metal oxides, nanocomposites [24], polymeric nanocomposites, microalgae strains, pyrite, clay minerals, and resins.

In the elimination of DS, carbon-based adsorbents such as AC derived from waste biomass have been utilized. AC stands out as one of the most successful adsorbents due to its widespread application, attributed to its high pore volume, significant permeability, developed internal porous structure, and abundance of surface functional groups [25]. The AD capacity of AC can be notably enhanced when impregnated with metals or metal oxides, owing to its extensive surface area. Gusain et al. [26] note its easy renewability and cost-effectiveness. Additionally, hydrothermal carbonization (HTC)—a thermochemical conversion method involving biowaste at room temperature and moderate pressure—has been highlighted by Zhang et al. [27]. This process produces biochar enriched with numerous oxygenated functional groups that aid in retaining incoming contaminants [28]. Moreover, the advantage of hydrothermal carbonization (HTC) lies in its minimal energy consumption, as it eliminates the necessity for pretreatment of biomass [29]. Despite the potential for increased energy usage in treating biomass over extended durations through HTC, the resultant yield is notably higher compared to other methods [30, 31].

In the DS-AD process on the activated carbon (AC) surface of sycamore balls, various factors were investigated, including pH, temperature, and adsorbent dosage. The adsorbent dose ranged from 2.5 mg/50 mL to 30 mg/50 mL at 25°C, while the IC of DS ranges from 10 to 50 mg/L. To assess the impact of AD temperature while maintaining a constant adsorbent dose (10 mg/50 mL), temperatures ranging from 25°C to 45°C were examined. The study by Avcu et al. [32] concluded that AC from sycamore balls serves as the best and cheapest adsorbent for DS-AD. Another approach involves saturating the surface of palm coconut AC with iron compound nanoparticles, utilizing pomegranate and leaves of *Moringa oleifera* extracts in an environmentally friendly preparation method to assess its AD capacity for DS [33].

Moreover, coconut shell-derived AC demonstrated a remarkable elimination rate of over 98% for DS under specific conditions, with an adsorbent dosage of Rads = 0.10 and a contact duration of 15 minutes [34], lasting up to 90 minutes. Additionally, AC derived from citrus industrial processing waste, through phosphoric acid activation, has been utilized for decontaminating water tainted with synthetic DS. Under ideal working conditions, the maximum DS adsorption capacity of AC was found to be 185.19 mg/g [35]. The primary aim of this research is to employ hydrothermal carbonization (HTC) as a cost-effective method to produce carbon from bamboo waste. The carbon obtained from HTC was then combined with ZnO synthesized via a sonochemical method. In laboratory settings, the resulting HTC-derived AC/ZnO composite was evaluated as a successful adsorbent for removing DS from water under ideal conditions. The incorporation of ZnO into the AC enhanced the microstructure, thereby increasing active sites and augmenting the adsorptive removal of harmful substances.

2. Experimental Protocol

2.1. Substances and Preparations. Analytical-grade materials were procured for all compounds, including concentrated H_2SO_4, Zn $(NO_3)_2$, and NaOH. A stock solution of 100 mg/L was prepared by dissolving 0.010 g of DS in 0.1 L of double-distilled water. Table 1 provides the characteristics of diclofenac sodium, and Figure 1 illustrates the structure of DS. The bamboo debris used as the carbon source in this study was sourced from discarded bamboo furniture obtained from a nearby warehouse in Chennai, India. Subsequently, the required solutions with the desired intensity were obtained from the base solution using the dilution law.

2.2. Preparation of Bamboo-Derived AC/ZnO. The bamboo underwent a thorough cleaning process, being rinsed three to four times with deionized water to ensure cleanliness. To eliminate moisture content, the bamboo was subjected to shade drying for three days. Subsequently, a mixer grinder was employed to pulverize the dry bamboo debris. The resulting mixture was then sieved using a shaking sieve with

Table 1: Characteristics of diclofenac sodium.

Parameter	Character/value
Commercial name	Diclofenac sodium, Voltaren, Diclac, etc.
Odour	Odourless
Nature	Crystalline
Colour	White or off-white
Molecular formula	$C_{14}H_{10}Cl_2NNaO_2$

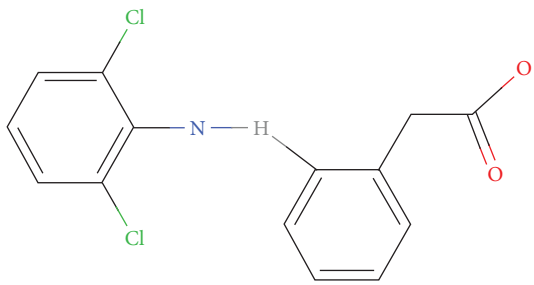

Figure 1: Structure of diclofenac sodium.

a 160 μm mesh size range to achieve various particle sizes. The dried bamboo waste was then subjected to heat treatment in an HTC autoclave maintained at 250°C for approximately three hours. After cooling, the liquid portion was drained, leaving behind the char resulting from the HTC process. This char underwent alkali activation by immersion in a NaOH solution for 8-9 consecutive hours. Neutralization was achieved through water washing or rinsing. The activated carbon (AC) was dried in a hot air oven until all moisture was completely removed.

For the creation of a 0.1N NaOH solution, 14.875 g of Zn $(NO_3)_2$ was mixed in 0.05 L of water to achieve a 1 M solution. This solution was kept in a 250 mL beaker and left at room temperature. While continuously stirring at 120 rpm using a magnetic stirrer, the prepared NaOH solution was slowly added drop by drop using a burette. This gradual addition resulted in a creamy white solution. Upon settling, a milky white precipitate of $Zn(OH)_2$ formed. The resulting precipitate was found to be alkaline. To neutralize it, the precipitate was rinsed with water three or four times. The pH was measured and recorded as 7.2. The collected Zn $(OH)_2$ was kept in a crucible and subjected to heating in a furnace at 500°C for approximately three hours, transforming it into ZnO. Subsequently, the resulting sludge was dried for 12 hr in a hot air oven.

During sonication, ZnO settled within the cracks of the activated carbon (AC) structure, causing surface fractures that enhanced its adsorption capabilities. This increases the removal percentage of DS in the AD process. In the experimental setup, a mixture comprising 50 mL of ethyl alcohol, 0.05 g of HTC-AC, and ZnO was subjected to sonication for 30 minutes. After settling, the dried material obtained from this process was identified as HTC-AC/ZnO (Figure 2).

2.3. Characterization of HTC-AC/ZnO. FTIR spectroscopy (Nicolet iS50, Thermo Fisher Scientific) was employed to determine the existence of surface functional groups on the produced materials and the mechanistic interaction of HTC-AC. The HTC-AC/ZnO surface morphology was analyzed using an SEM operating at 10 kV (JEOL/EO—JCM 6000 plus) before the materials were gold flashed. The PANALYTICAL X'Pert PRO X-ray diffractometer was used to capture XRD patterns. At a scanning rate of 10 min^{-1}, Cu Kα ($\lambda = 1.540$ Å) radiation was used in the 2Θ range of 10–80°. Using a Micromeritics 2000 device, N_2 adsorption at −196°C was measured to calculate the BET surface area. Then, using the cumulative nitrogen adsorption-desorption as a basis, the pore volumes were determined utilizing the BJH (Barrett–Joyner–Halenda) technique.

2.4. Adsorption Studies for the Removal of DS by AC/ZnO. In a typical AD procedure, measured quantities of HTC-AC/ZnO (0.5–4 g/L) were mixed with successive 100 mL glass vials containing 50 mL of DS solutions with IC ranging from 50 mg/L to 250 mg/L. These mixtures were agitated at ambient temperature in a thermostatic shaker incubator at 120 rpm. The filtrate was filtered using a 0.22 μm nylon membrane syringe filter and collected in a syringe for subsequent quantitative analysis. Quantitative testing of DS was conducted utilizing a UV double-beam spectrophotometer set at its largest wavelength of 275 nm. Each study was run three times, and analysis was done using the mean results. The following formulas were employed to calculate the percentage of DS removed and the quantities of DS adsorbed per unit mass of HTC-AC/ZnO:

$$\text{Removal efficiency } (\%) = \frac{(C_0 - C_t)}{C_0} \times 100, \quad (1)$$

where C_0 is the IC of DS (in mg/L) and C_t is the concentration of DS at any time "t" (in mg/L).

The quantities of DS adsorbed per unit mass of HTC-AC/ZnO at any time "t" (q_t in mg/g) and at equilibrium (q_e in mg/g) were determined by utilizing the expression:

$$q_t = \frac{(C_0 - C_t) \times V}{m}, \quad (2)$$

$$q_e = \frac{(C_0 - C_e) \times V}{m}, \quad (3)$$

where V is the volume of the solution (in L), m is the mass of the HTC-AC/ZnO (in g), and C_e is the equilibrium concentration of DS in the solution (in mg/L).

2.5. Thermodynamic Studies. To characterize the thermodynamic nature of the AD process of DS, thermodynamic activation parameters involving ΔH° (enthalpy), ΔS°

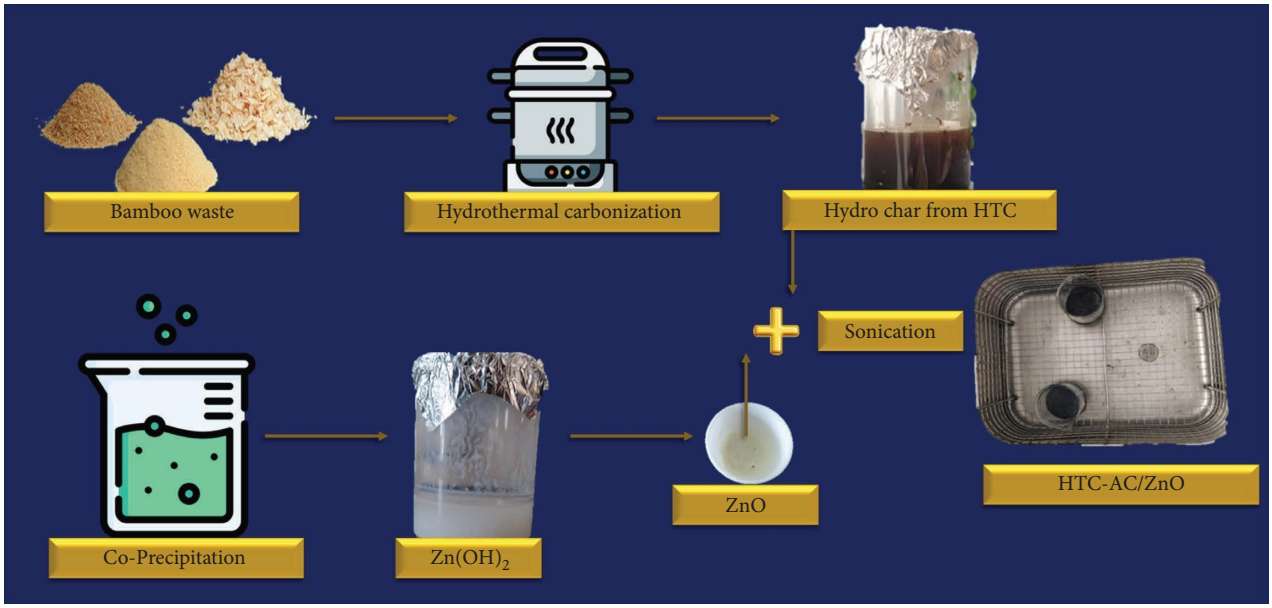

Figure 2: Methodology to prepare the HTC-AC/ZnO.

(entropy), and ΔG° (Gibbs free energy) were computed. ΔG° was determined using equation (5).

$$K_C = \frac{C_{ae}}{C_e}, \tag{4}$$

$$\Delta G^\circ = -\mathrm{RTln}\,(\mathrm{Kc}), \tag{5}$$

$$\mathrm{Log}K_c = \frac{\Delta S^0}{2.303R} - \frac{\Delta H^0}{2.303\mathrm{RT}}. \tag{6}$$

2.6. Adsorption Isotherm Studies. The distribution of the adsorbate among the HTC-AC/ZnO and DS solution upon reaching adsorption equilibrium can be elucidated using AD isotherms, which play a crucial role. In this research, three adsorption isotherm models—the Freundlich isotherm model (FIM), Temkin isotherm model (TIM), and Langmuir isotherm model (LIM)—were employed to characterize the DS-AD process and delineate the distribution of DS in aqueous solution and on the surface of HTC-AC/ZnO during AD equilibrium. Table 2 presents the nonlinear mathematical formulas used to determine the adsorption isotherm parameters.

2.7. Adsorption Kinetic Studies. A high AD rate and substantial AD capacity are essential characteristics for the practical industrial uses of an adsorbent in WWT facilities. The kinetic study of DS-AD on HTC-AC/ZnO was conducted over a duration ranging from 0 to 210 minutes. Models including pseudo-first order model (PFOM), pseudo-second order model (PSOM), and intraparticle diffusion model (IPDM) were studied to fit the data in AD kinetics from DS-AD tests. The formulas for these models are presented in Table 3.

3. Outcome and Discussion

3.1. Adsorbent Characterization. XRD analysis was conducted to find the crystalline structures of HTC-AC, ZnO, and HTC-AC/ZnO, as illustrated in Figures 3(a)–3(c), respectively. The AC derived from HTC exhibits a broad peak between 20 and 30°, exactly around $\theta = 23.53°$, without a distinct graphitic structure at its summit. This XRD pattern at 23.53° signifies the amorphous state of carbon [42]. Figure 3(a) indicates that the peak intensity at 23.53° is higher than that at 42.59°. The heightened peak intensity at 23.53° is suggestive of a stack of parallel aromatic layers, while the lower intensity at 42.59° corresponds to the regular arrangement of a single-layer segment. ZnO displayed distinct diffraction peaks at various angles, notably at $2\theta = 33.23°$, 34.52°, 36.43°, 47.62°, 56.71°, 63.03°, and 68.12°, with the most prominent peak observed at 36.12° as shown in Figure 3(b). This pattern confirms the absence of any visible impurities or multiple phases in ZnO, indicating its exceptional purity [43]. In contrast, the XRD pattern of AC-ZnO exhibited more peaks in comparison to ZnO and AC. Notable peaks were observed at $2\theta = 24.03°$, 31.70°, 34.51°, 36.38°, 47.49°, 56.72°, 62.98°, 67.99°, 72.85°, and 77.37°. Two more prominent peaks formed at $2\theta = 24.03°$ and $2\theta = 36.98°$ (seen in Figure 3(c)), with the peak at $2\theta = 24.03°$ indicating the presence of AC and the peak at $2\theta = 36.98°$ indicating the presence of ZnO [44]. This suggests the incorporation of ZnO into the outer layer of AC, leading to these distinctive peaks. The hexagonal wurtzite structure is evident in the HTC-AC/ZnO composite.

A nitrogen AD isotherm at 77 K was conducted to comprehensively assess the porous characteristics of the synthesized HTC-AC/ZnO material. The resulting isotherm, depicted in Figure 4(a), includes the BJH pore-size distribution plot (Figure 4(b)). HTC-AC/ZnO exhibited a combined type II and IV AD-desorption isotherm, indicating its

Table 2: Adsorption isotherm models and nonlinear equations.

Isotherm model	Equation	Parameters	Reference
LIM	$q_e = (q_m K_L C_e)/(1 + K_L C_e)$	K_L: Langmuir adsorption constant (L/mg)	[36]
FIM	$q_e = K_F C_e^{1/n}$	K_F: Freundlich constant (mg/g) $(L/mg)^{1/n}$ n: Freundlich exponent	[37]
TIM	$q_e = B \ln(AC_e)$	B: RT/b corresponds to the enthalpy of adsorption b corresponds to the Temkin constant, associated with the heat of adsorption (measured in J/mol) T denotes the temperature in Kelvin R represents the universal gas constant A represents the binding constant at equilibrium, signifying the maximum binding energy (measured in L/g)	[38]

Table 3: Adsorption kinetics and nonlinear equations.

Kinetic model	Equation	Parameters	Reference
PFOM	$q_t = q_e(1 - \exp(-k_1 t))$	k_1: PFOM rate constant (min^{-1})	[39]
PSOM	$q_t = (q_e^2 k_2 t)/(1 + q_e k_2 t)$	k_2: PSOM rate constant (g mg^{-1}·min^{-1})	[40]
IPDM	$q_t = k_p t^{(1/2)} + C$	k_p: IDPM rate constant (mg g^{-1}·min^{-1}) C: intercept reflecting the boundary layer thickness	[41]

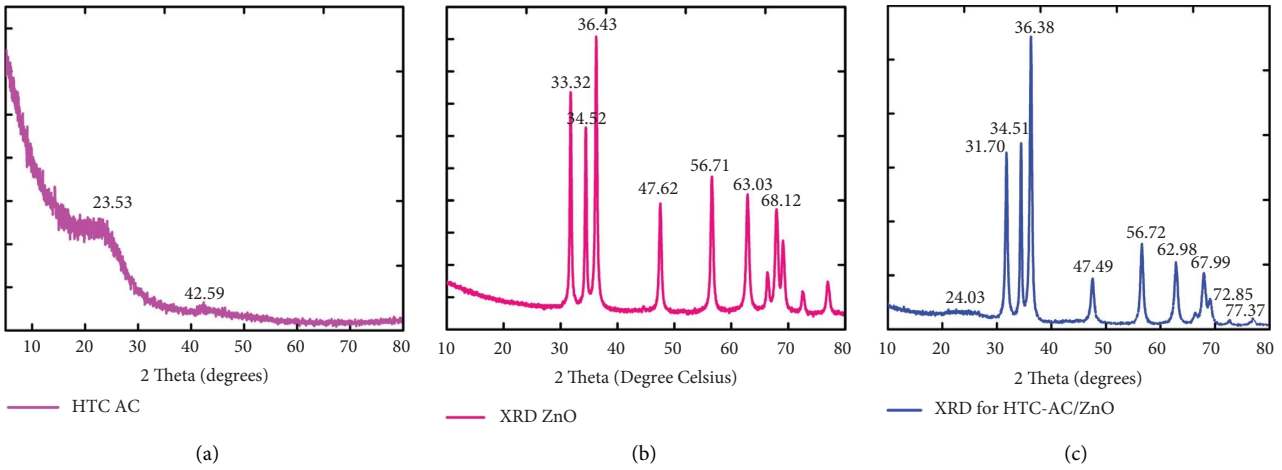

Figure 3: XRD pattern of (a) HTC-AC, (b) ZnO, and (c) HTC-AC/ZnO; y-axis is in intensity (a.u).

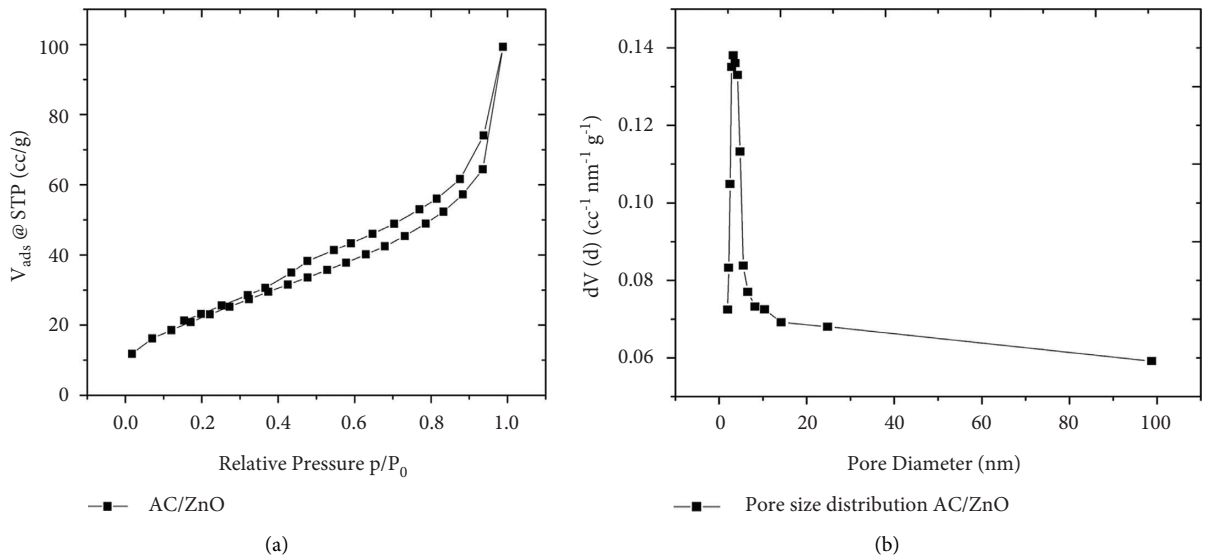

Figure 4: BET analysis. (a) N_2-AD isotherm of HTC-AC/ZnO. (b) Pore size distribution of HTC-AC/ZnO.

integrated nature [45]. The hysteresis loop observed in the isotherm, characterized by a broad condensation step in the medium-to-high region and a flatter section at the center (relative pressure, $p/P^\circ = 0.1–1.0$), strongly shows the prevalence of macropores and mesopores in HTC-AC/ZnO. The BJH pore-size distribution plot (Figure 4(b)) further corroborated this observation, revealing the presence of mesopores ranging in size from 2 to 50 nm and micropores with a mean size of roughly 2.848 nm. The BET surface area of HTC-AC/ZnO was measured at 89.124 m^2/g. Analysis revealed a micropore volume of 0.008 cm^3/g and a larger mesopore volume of 0.145 cm^3/g, resulting in a total pore volume of 0.153 cm^3/g. This indicates a prevalence of mesoporous structure over microporous structure, supported by the pore volume and average pore diameter data. The presence of a higher proportion of mesopores compared to micropores suggests favorable conditions for high diffusion rates and effective capture of DS molecules upon interaction with the active AD sites on the outer layer of HTC-AC/ZnO [46].

Figure 5 displays the resulting FTIR spectrum obtained from the HTC-AC sample, aiming to identify the surface's functional groups. The carbon framework of bamboo comprises intricate blends of polysaccharides, notably rich in O-H and C=O groups found in hemicellulose, cellulose, and lignin. After heat treatment, the resulting biochar underwent infrared spectrum analysis spanning 400 to 4000 cm^{-1} to discern structural changes. The spectra exhibit a widened intensity at 3564 cm^{-1}, corresponding to OH stretching vibrations, indicative of decreased carbonization [47]. Additionally, a brief peak at 2788 cm^{-1} is attributed to the stretching vibrations of the carbonyl aliphatic C-H group. The identification of AC formation through aromatization suggests the dehydrogenation of existing cyclic compounds, resulting in the existence of aliphatic C groups in the material. The synthesis of aromatic rings during the hydrothermal process is evidenced by the strength of aromatic ring stretching vibrations, notably observed at around 1521 cm^{-1} [48]. Additionally, the FTIR spectrum exhibited a characteristic fingerprint region with a broad and shallow intensity at 1069 cm^{-1}. This intensity corresponds to carbonyl groups, which are attributed to the formation of C=O groups originating from the dehydrogenation of one or more saccharide molecules.

Figure 6 exhibits the structure and morphology of HTC-AC impregnated with ZnO. Hydrochars produced through hydrothermal carbonization (HTC) are known to display sphere-shaped formations, suggesting the carbon's spherical structure or the presence of smooth-surfaced sphere aggregates. These spheres were observed to have diameters ranging from a few microns. Furthermore, the aggregation of these spheres into clusters suggests the accumulation of hydrolysis products derived from bamboo polymers [49]. These products are likely composed of polyaromatic structures, featuring hydrophobic (less reactive) groups concentrated in the core and hydrophilic (more reactive) groups on the surface. Key processes such as polymer aromatization and dehydration contribute significantly to the creation of polyaromatic structures within the HTC-AC/ZnO. The notable characteristics of this material, including its substantial pore volume (0.153 cm^3/g) and extensive surface area (89.124 m^2/g), are attributed to the existence of active sites. These features play an important role in facilitating the effective elimination of DS from contaminated effluents.

3.2. Adsorption Studies. The AD capacity of the obtained HTC-AC/ZnO material was systematically assessed in a batch process for the elimination of DS from contaminated effluents. DS was selected as the model PC due to its widespread use as an NSAID, its ubiquitous presence in global wastewater systems, its significant toxicity towards various organisms, high water solubility, and prolonged persistence in aquatic environments [12].

3.2.1. Effect of HTC-AC/ZnO Dosage on DS Removal. Several studies were conducted using different quantities of HTC-AC/ZnO, ranging from 0.5 to 4 g/L, under specific conditions: pH 2, 50 mg/L DS initial concentration, and a 30-minute adsorption duration at 303 K. The variation in the adsorption capacity and efficiency of HTC-AC/ZnO as a function of its dose is depicted in Figure 7. The figure illustrates a notable increase in adsorption efficiency as the adsorbent concentration reaches 4 g/L. This rise in efficiency is attributed to the higher availability of accessible binding active sites, indicating an improved adsorption capacity at the higher adsorbent concentration. The observed increase in adsorption efficiency is likely a result of the rise in surface active sites of HTC-AC/ZnO. These findings suggest that the optimal adsorbent concentration for our experimental conditions was determined to be 4 g/L of HTC-AC/ZnO, which will be utilized in subsequent research [50].

3.2.2. Effect of DS-IC on DS Removal. Multiple tests were conducted using different initial concentrations (IC) of DS, ranging from 50 to 250 mg/L, under specific conditions: pH 2, HTC-AC/ZnO dosage of 4 g/L, and a 30-minute adsorption duration at 303 K. Figure 8 illustrates the variation in the adsorption capacity and efficiency of HTC-AC/ZnO in relation to DS's initial concentration (IC). The observed decrease in adsorption efficiency with increasing DS concentration can be attributed to competitive adsorption among sorbate molecules. As DS concentration in the solution increases, more DS ions can access the available surface sites of HTC-AC/ZnO. The maximum removal percentage was 99.38%, obtained at 50 mg/L. Consequently, the higher concentration drives a stronger force to overcome the mass transfer barrier for DS between the DS solution and the HTC-AC/ZnO, resulting in a decrease in the elimination of DS [51].

3.2.3. Impact of Contact Time on DS Removal. The removal of DS from a water-based solution was assessed at varying contact times and initial concentrations (ICs) of DS, ranging from 50 to 250 mg/L, at pH 2 and 303 K, as depicted in Figure 9. The results obtained from the adsorption process of DS on HTC-AC/ZnO indicate that prolonged contact durations enhance the adsorption mechanism. The adsorption capacity (AD) of DS onto HTC-AC/ZnO demonstrated an accelerated phase during the initial half hour, reaching optimal values for five distinct ICs of DS. Subsequent increases in contact time marginally affected the proportion of DS removal [52, 53].

The larger surface area of HTC-AC/ZnO initially contributed to its enhanced capacity for absorbing DS ions. The rate of movement of adsorbed DS ions from the outermost layer to the inner part of HTC-AC/ZnO governs the speed of adsorption once DS forms a monolayer and saturates the potential of HTC-AC/ZnO. This process is crucial as only a small number of efficient adsorption sites are available, allowing each binding site to accommodate a single ion within this monolayer. As the surface reaches saturation, there is competition for a finite number of binding sites. This competition leads to an initial rapid adsorption of DS onto the HTC-AC/ZnO surface, followed by a slower rate. The existing DS in the

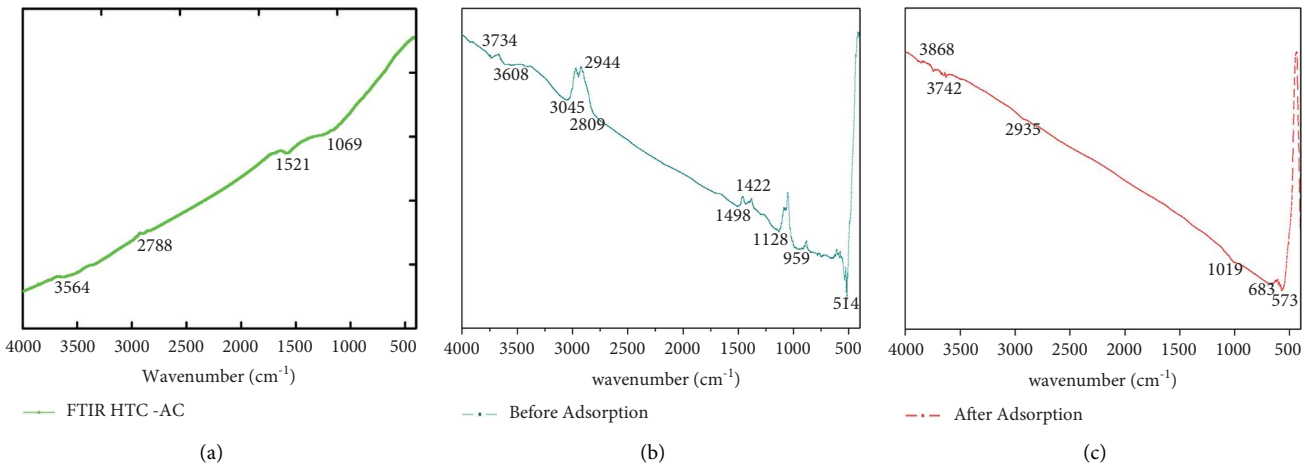

Figure 5: FTIR spectrum for (a) HTC-AC, (b) HTC-AC/ZnO before adsorption, and (c) HTC-AC/ZnO after adsorption; *y*-axis is in transmittance (%).

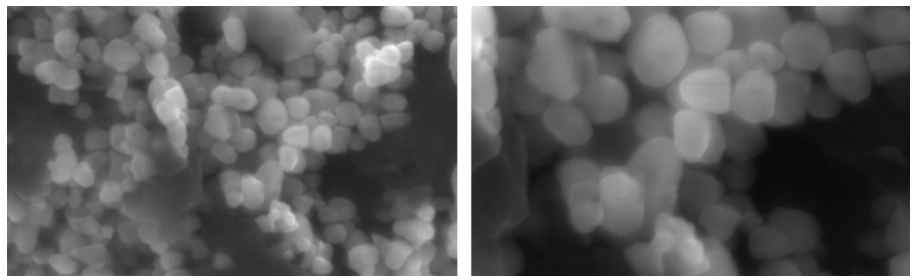

Figure 6: SEM morphology for HTC-AC/ZnO.

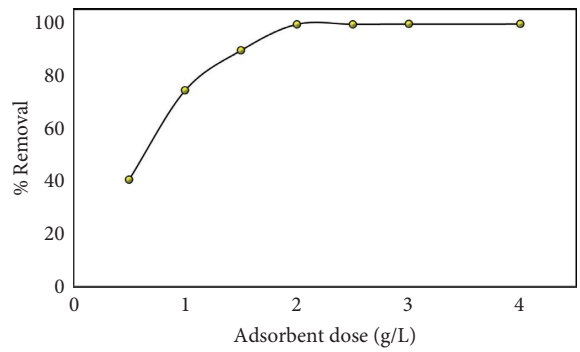

Figure 7: Influence of HTC-AC/ZnO on DS removal (DS-IC: 50 mg/L; time: 30 min; pH: 2; temp.: 303 K).

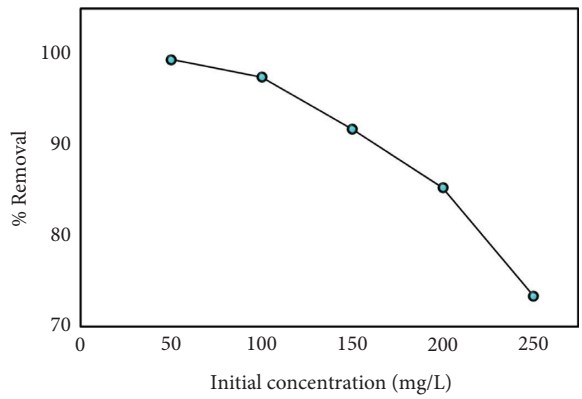

Figure 8: Influence of IC of DS-on-DS removal (AC/ZnO dose: 4 g/L; pH: 2; time: 30 min; temp.: 303 K).

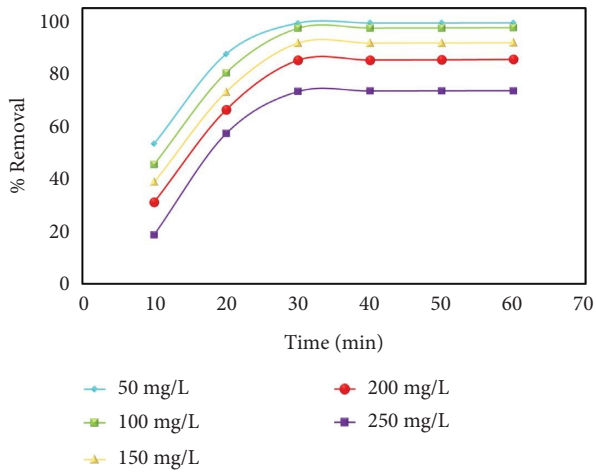

Figure 9: Effect of time on DS removal (AC/ZnO dose: 4 g/L; IC-DS: 50–250 mg/L; pH: 2; and temp.: 303 K).

sample enhances the competition for these binding sites, contributing to the slower adsorption rate later in the process.

3.2.4. Impact of pH on DS Removal. Figure 10 illustrates the impact of the starting solution's pH on DS removal. To adjust the initial pH levels, 0.1 M solutions of HCl or NaOH were added. The percentage clearance of DS decreased from 99.38% at pH 2 to 18.39% at pH 12, as evident from the figure. The fluctuation in adsorption efficiency with pH can be attributed to the electrostatic attraction between HTC-AC/ZnO and DS. As pH values increase, the outer layers of HTC-AC/ZnO gradually lose positive charges, transitioning to a more negative state.

At low pH, the positive charge on the HTC-AC/ZnO surface was high, leading to a stronger interaction between the HTC-AC/ZnO surface and the π-electron cloud of the DS molecule. At higher pH, the positive charge on the HTC-AC/ZnO surface decreases, and OH- ions also compete with the DS molecules for adsorption on the active sites, resulting in a reduction in the adsorption efficiency of HTC-AC/ZnO. At neutral pH, only a slight influence of H+ or OH- ions was observed on the HTC-AC/ZnO surface; therefore, almost constant adsorption of DS was observed [54].

The significant electrostatic interaction between anions and positively charged sites (H+) on HTC-AC/ZnO primarily accounts for its substantial adsorption capacity at low pH levels. However, at alkaline pH, the abundance of OH- ions introduces competition for the same adsorption sites, potentially reducing the adsorption of DS ions [55].

3.2.5. Effect of Temperature on DS Removal. Figure 11 illustrates the correlation between temperature variations and the efficiency of DS removal by HTC-AC/ZnO. The removal efficiency of DS notably decreases with increasing temperatures, showing reductions from 97.38% to 92.41% at 50 mg/L, 97.35% to 92.36% at 100 mg/L, 91.73% to 85.33% at 150 mg/L, 85.27% to 79.22% at 200 mg/L, and 73.31% to

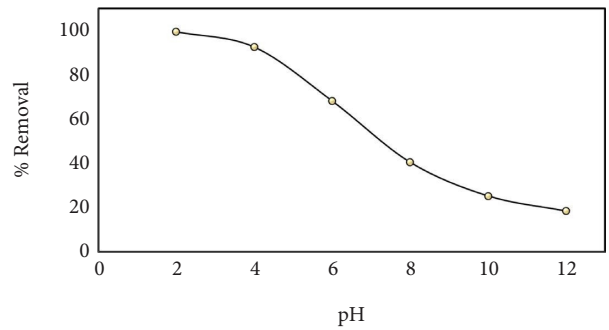

Figure 10: Effect of pH on DS removal (AC/ZnO dose: 4 g/L; time: 30 min; IC-DS: 50 mg/L; temp.: 303 K).

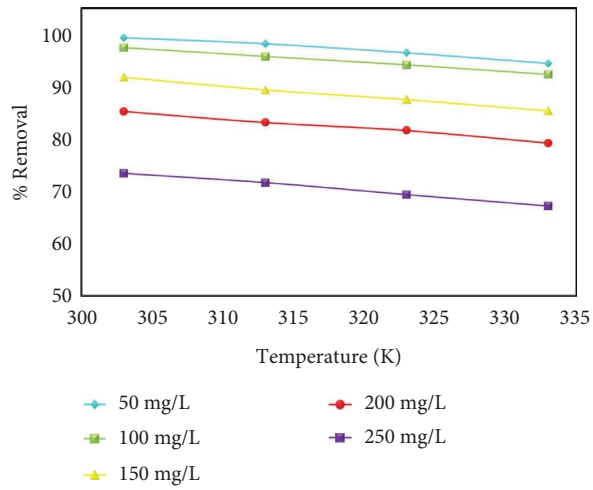

Figure 11: Effect of temperature on DS removal (AC/ZnO dose: 4 g/L; time: 30 min; IC-DS: 50–250 mg/L; pH: 2).

67.21% at 250 mg/L. This observation supports the conclusion of an exothermic nature in the DS adsorption process, indicating that adsorbing DS at lower temperatures is advantageous. Additionally, this characteristic is corroborated by the negative enthalpy energy (ΔH°) values [56].

3.3. Thermodynamic Studies. The plotting of log Kc against 1/T resulted in a linear relationship (Figure 12). Enthalpy change and entropy change parameters were derived from the gradient and intercept of the graph, respectively, and subsequently added to Table 4 alongside the remaining parameters. The adsorption-desorption process is evidently exothermic, indicated by $\Delta H^\circ < 0$ in the table. Moreover, $\Delta S^\circ < 0$ suggests a decrease in unpredictability at the HTC-AC/ZnO/DS solution interface. The adsorption process appears both spontaneous and feasible, as evidenced by the negative values of ΔG°. Additionally, a decrease in ΔG° with an increase in temperature suggests a strong preference for the AD of DS. Moreover, the ΔG° values being less than −40 kJ/mol indicate that a physisorption process might be responsible for the interactions occurring between the surface of HTC-AC/ZnO and DS.

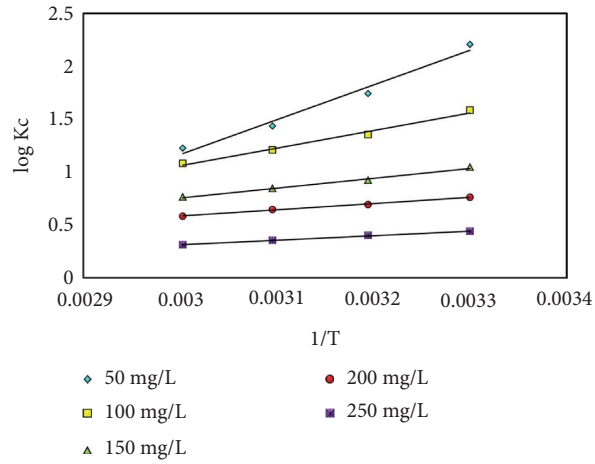

Figure 12: Thermodynamic studies on DS removal.

Table 4: Thermodynamic parameters for the DS removal by HTC-AC/ZnO.

IC-DS (mg/L)	ΔH° (kJ/mol)	ΔS° (J/mol/K)	ΔG° (kJ/mol)			
			303 K	313 K	323 K	333 K
50	−62.8	−166.101	−12.79	−10.44	−8.88	−7.83
100	−31.92	−75.4972	−9.18	−8.12	−7.47	−6.90
150	−17.80	−38.9261	−6.06	−5.53	−5.22	−4.87
200	−11.38	−22.9957	−4.42	−4.15	−4.01	−3.70
250	−8.34	−19.0514	−2.55	−2.41	−2.19	−1.99

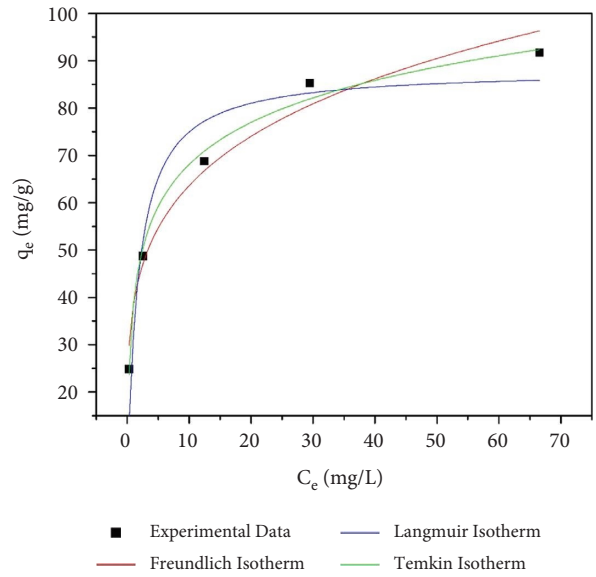

Figure 13: Adsorption isotherm studies on DS removal.

3.4. Adsorption Isotherms. While maintaining constant values for pH, adsorbent dose (2 and 4 g/L), and contact duration (30 minutes) and varying IC-DS, we examined its impact on the sorption process. Figure 13 presents a schematic representation illustrating the change in adsorption (AD) capacity and efficiency concerning IC-DS. To analyze DS equilibrium AD onto HTC-AC/ZnO, we employed LIM, FIM, and TIM. The computed parameters for these models using Origin pro 8.5 are shown in Table 5. The correlation coefficients (R^2) obtained from the utilized isotherm models generally fall within the range of 0.88 to 0.99. Notably, TIM exhibits the highest R^2 value, suggesting a consistent interaction among adsorbate molecules on the surface. Furthermore, this model indicates a linear decrease in the heat of AD corresponding to surface coverage, highlighting the presence of heterogeneous sites with varying AD energies.

Table 5: Isotherm variables in different isotherms for the DS removal by HTC-AC/ZnO.

Isotherm model	Parameters	R^2
Langmuir	q_m = 88.15 K_L = 0.56	0.88647
Freundlich	K_F = 38.43 n = 4.57	0.96718
Temkin	A (L/mg): 20.30 B: 12.81 b (kJ/mol): 0.196	0.99077

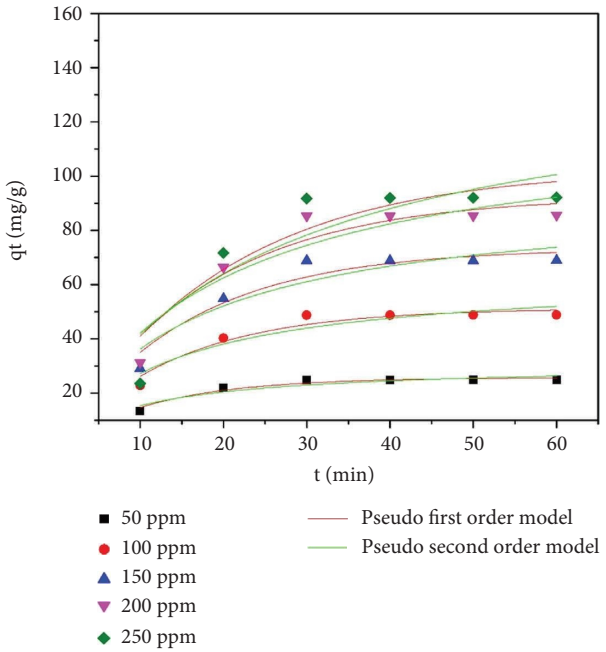

Figure 14: PFOM and PSOM for DS removal by HTC-AC/ZnO.

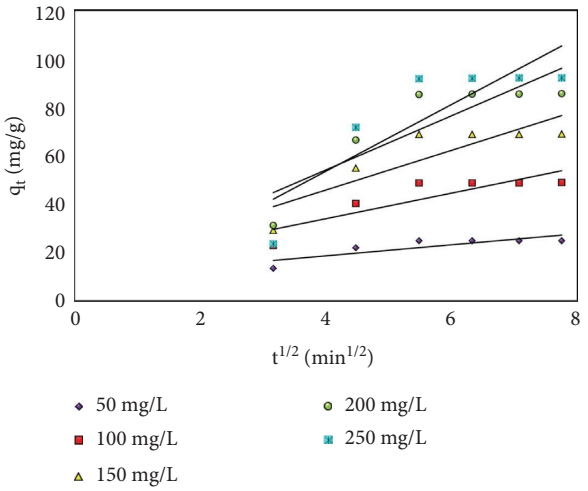

Figure 15: IPDM for DS removal by HTC-AC/ZnO.

3.5. Adsorption Kinetics. Adsorption studies were conducted at various time intervals while keeping the other process variables constant at optimal levels (pH around 2, adsorbent dose maintained at 4 g/L, and initial concentrations of DS between 50 and 250 mg/L) to investigate the influence of contact duration on the adsorption (AD) capacity. The

Table 6: Kinetic model and its parameters for the DS removal by HTC-AC/ZnO.

Type of adsorption kinetics	Parameters	Units	Concentration (mg/L)				
			50	100	150	200	250
	q_e, exp	mg/g	25.21	49.11	69.07	86.23	92.27
PFOM	k_1	min^{-1}	0.08477	0.07144	0.06479	0.05832	0.05068
	q_e	mg/g	25.69371	51.25704	73.32552	92.64226	102.89611
	R^2	—	0.94554	0.93325	0.91824	0.89428	0.8292
PSOM	k_2	$g{\cdot}mg^{-1}{\cdot}min^{-1}$	0.00326	0.00118	$6.83691E-4$	$4.40547E-4$	$2.97765E-4$
	q_e	mg/g	30.63476	63.48749	93.05429	121.01329	140.57596
	R^2	—	0.8588	0.86397	0.85626	0.83927	0.78243

Table 7: IPDM and its variables for the DS removal by HTC-AC/ZnO.

Type of adsorption kinetics	Parameters	Units	Concentration (mg/L)				
			50	100	150	200	250
IPDM	K_3	$mg/g{\cdot}min^{0.5}$	2.2788	5.3086	8.2069	$y = 11.213$	13.825
	C	mg/g	9.4432	12.713	13.037	9.1823	−1.7577
	R^2	—	0.7087	0.7434	0.7526	0.7545	0.7303

Table 8: Comparison of DS removal with various adsorbents.

Adsorbent	Adsorption capacity/percentage removal of DS	Reference
Isabel grape (*Vitis labrusca* × *Vitis vinifera*) bagasse	11.15 mg/g	[57]
Commercial organoclay	0.133 mmol/L	[58]
Moringa oleifera pod	60.805 mg/g	[59]
Babassu coconut activated carbon	71.150 mg/g	[59]
Bentonite polyureaformaldehyde	35.71 mg/g	[60]
Graphene	59.67 mg/g	[61]
Magnetic amine-functionalized chitosan	469.48 mg/g	[62]
HTC-AC/ZnO	88.15 mg/g	Current study

Table 9: Cost analysis of HTC-AC/ZnO.

HTC-AC/ZnO	Components	Net price (INR)
Laboratory prepared	Materials	48.3
	Operation	45
	Manpower	75
	Other overhead charges	25
	Total	193.3

analysis of Figures 14 and 15 using the PFOM, PSOM, and IPDM was plotted using Origin pro 8.5, aimed to determine the kinetic order and AD mechanism of DS on HTC-AC/ZnO in this research. The calculated rate constants, maximum quantity adsorbed, and R^2 from the relevant models are listed in Tables 6 and 7. Notably, the PFOM exhibited an exceptionally high R^2 value, nearly reaching unity. Moreover, its calculated q_e value of 25.69 mg/g showed close agreement with the experimental value of 25.21 mg/g. These findings strongly suggest that the PFOM accurately represents the kinetics of DS adsorption by HTC-AC/ZnO and stands out as the most suitable kinetic model for depicting this process. Table 8 gives the comparison of DS removal by various adsorbents.

4. Cost Analysis

For the treatment of commercial water and wastewater, the adsorbent's cost-effectiveness is a crucial component. Material, labour, and operating costs were added to additional overhead fees to get the total cost of the synthesized HTC-AC/ZnO. The primary expenses for raw materials included bamboo, H_2SO_4, Zn $(NO_3)_2$, NaOH, and DS. On the other hand, magnetic stirring, autoclave synthesis, centrifugal washing, and drying incurred power expenditures. As shown in Table 9, the cost analysis of synthesized HTC-AC/ZnO powder was computed. According to the cost analysis results, the cost of HTC-AC/ZnO manufactured in a laboratory was Rs. 193.3 g^{-1}.

5. Conclusion

In this study, we synthesized low-cost porous activated carbon (HTC-AC/ZnO) using bamboo as a carbon source via hydrothermal carbonization (HTC) and subsequently impregnated it with ZnO. Our aim was to determine the adsorptive efficiency of this resulting material in eliminating DS from polluted water. HTC-AC/ZnO exhibited a high specific surface area and total pore volume, measuring 89.124 m^2/g and 0.153 cm^3/g, respectively, indicating an organized micro/mesoporous morphology. The adsorption isotherm analyses revealed a substantial binding capacity of 88.15 mg/g for the adsorption of DS onto HTC-AC/ZnO, suggesting that the adsorption behavior can be accurately interpreted using the TIM model. Moreover, the adsorption kinetics exhibited rapid adsorption rates, aligning well with the PFOM. Notably, the substantial removal efficiency of 99.38% of DS from the aqueous solution using HTC-AC/ZnO is remarkable. With its straightforward production process, exceptional adsorption capacity, and swift adsorption rates, HTC-AC/ZnO emerges as a praiseworthy adsorbent for efficiently purifying DS-contaminated wastewater.

Data Availability

Data are available on request.

Ethical Approval

This article does not contain any studies involving animal or human participants performed by any of the authors.

Conflicts of Interest

The authors declare that they have no conflicts of interest.

Authors' Contributions

Kilaru Harsha Vardhan was responsible for investigation, methodology, supervision, and original draft preparation. P. Senthil Kumar was responsible for conceptualization, validation, and supervision. Hrishitha Sree and B. Senthil Rathi were responsible for investigation, methodology, data curation, and original draft preparation.

References

[1] S. Esplugas, D. M. Bila, L. G. T. Krause, and M. Dezotti, "Ozonation and advanced oxidation technologies to remove endocrine-disrupting chemicals (EDCs) and pharmaceuticals and personal care products (PPCPs) in water effluents," *Journal of Hazardous Materials*, vol. 149, no. 3, pp. 631–642, 2007.

[2] M. l. Farré, S. Pérez, L. Kantiani, and D. Barceló, "Fate and toxicity of emerging pollutants, their metabolites and transformation products in the aquatic environment," *TrAC, Trends in Analytical Chemistry*, vol. 27, no. 11, pp. 991–1007, 2008.

[3] T. Liu, C. O. Aniagor, M. I. Ejimofor et al., "Technologies for removing pharmaceuticals and personal care products (PPCPs) from aqueous solutions: recent advances, performances, challenges and recommendations for improvements," *Journal of Molecular Liquids*, vol. 374, 2023.

[4] M. J. Sampaio, A. R. Ribeiro, C. M. Ribeiro et al., "A technological approach using a metal-free immobilized photocatalyst for the removal of pharmaceutical substances from urban wastewaters," *Chemical Engineering Journal*, vol. 459, 2023.

[5] S. D. Kayode-Afolayan, E. F. Ahuekwe, and O. C. Nwinyi, "Impacts of pharmaceutical effluents on aquatic ecosystems," *Scientific African*, vol. 17, 2022.

[6] L. Wang, Y. Xu, T. Qin et al., "Global trends in the research and development of medical/pharmaceutical wastewater treatment over the half-century," *Chemosphere*, vol. 331, 2023.

[7] M. Al Aukidy, P. Verlicchi, A. Jelic, M. Petrovic, and D. Barcelò, "Monitoring release of pharmaceutical compounds: occurrence and environmental risk assessment of two WWTP effluents and their receiving bodies in the Po Valley, Italy," *Science of the Total Environment*, vol. 438, pp. 15–25, 2012.

[8] V. Acuña, A. Ginebreda, J. R. Mor et al., "Balancing the health benefits and environmental risks of pharmaceuticals: diclofenac as an example," *Environment International*, vol. 85, pp. 327–333, 2015.

[9] I. Boarescu, R. M. Pop, P. M. Boarescu et al., "Ginger (zingiber officinale) root capsules enhance analgesic and antioxidant efficacy of diclofenac sodium in experimental acute inflammation," *Antioxidants*, vol. 12, no. 3, p. 745, 2023.

[10] Y. Zhang, S. U. Geißen, and C. Gal, "Carbamazepine and diclofenac: removal in wastewater treatment plants and occurrence in water bodies," *Chemosphere*, vol. 73, no. 8, pp. 1151–1161, 2008.

[11] A. C. Mehinto, "Impacts of the human pharmaceutical diclofenac in the aquatic environment," 2009, https://ore.exeter.ac.uk/repository/bitstream/handle/10036/94969/MehintoA.pdf?sequence=2&isAllowed=y.

[12] L. Lonappan, S. K. Brar, R. K. Das, M. Verma, and R. Y. Surampalli, "Diclofenac and its transformation products: environmental occurrence and toxicity-a review," *Environment International*, vol. 96, pp. 127–138, 2016.

[13] J. M. Angosto, M. J. Roca, and J. A. Fernández-López, "Removal of diclofenac in wastewater using biosorption and advanced oxidation techniques: comparative results," *Water*, vol. 12, no. 12, p. 3567, 2020.

[14] D. Cherik, M. Benali, and K. Louhab, "Occurrence, ecotoxicology, removal of diclofenac by adsorption on activated carbon and biodegradation and its effect on bacterial community: a review," *World Scientific News*, vol. 10, pp. 116–144, 2015.

[15] P. Iovino, S. Chianese, S. Canzano, M. Prisciandaro, and D. Musmarra, "Photodegradation of diclofenac in wastewaters," *Desalination and Water Treatment*, vol. 61, no. 2, pp. 293–297, 2017.

[16] I. Vergili, "Application of nanofiltration for the removal of carbamazepine, diclofenac and ibuprofen from drinking water sources," *Journal of Environmental Management*, vol. 127, pp. 177–187, 2013.

[17] K. P. M. Licona, L. D. O. Geaquinto, J. V. Nicolini et al., "Assessing potential of nanofiltration and reverse osmosis for removal of toxic pharmaceuticals from water," *Journal of Water Process Engineering*, vol. 25, pp. 195–204, 2018.

[18] M. Rosset, L. W. Sfreddo, G. E. N. Hidalgo, O. W. Perez-Lopez, and L. A. Feris, "Adsorbents derived from

hydrotalcites for the removal of diclofenac in wastewater," *Applied Clay Science*, vol. 175, pp. 150–158, 2019.

[19] J. O. Ighalo and A. G. Adeniyi, "Mitigation of Diclofenac pollution in aqueous media by adsorption," *ChemBioEng Reviews*, vol. 7, no. 2, pp. 50–64, 2020.

[20] Q. Li, F. Wang, Y. Wang et al., "Adsorption behavior and mechanism analysis of siloxane thickener for CO2 fracturing fluid on shallow shale soil," *Journal of Molecular Liquids*, vol. 376, 2023.

[21] I. Alessandretti, C. V. T. Rigueto, M. T. Nazari, M. Rosseto, and A. Dettmer, "Removal of diclofenac from wastewater: a comprehensive review of detection, characteristics and tertiary treatment techniques," *Journal of Environmental Chemical Engineering*, vol. 9, no. 6, 2021.

[22] A. A. Haghgoo, M. Cheraghi, S. Sobhanardakani, B. Lorestani, and V. Izadkhah, "Preparation of AC/KOH and AC/Fe3O4/ZnO nanocomposite from waste rice straw for the removal of cyclophosphamide from aqueous solutions," *Toxin Reviews*, vol. 42, no. 1, pp. 275–284, 2023.

[23] F. Wang, Z. Xiao, X. Liu et al., "Strategic design of cellulose nanofibers@ zeolitic imidazolate frameworks derived mesoporous carbon-supported nanoscale CoFe2O4/CoFe hybrid composition as trifunctional electrocatalyst for Zn-air battery and self-powered overall water-splitting," *Journal of Power Sources*, vol. 521, 2022.

[24] S. Sobhan Ardakani, M. Cheraghi, A. Jafari, and R. Zandipak, "PECVD synthesis of ZnO/Si thin film as a novel adsorbent for removal of azithromycin from water samples," *International Journal of Environmental Analytical Chemistry*, vol. 102, no. 17, pp. 5229–5246, 2022.

[25] M. Raninga, A. Mudgal, V. K. Patel, J. Patel, and M. Kumar Sinha, "Modification of activated carbon-based adsorbent for removal of industrial dyes and heavy metals: a review," *Materials Today: Proceedings*, vol. 77, pp. 286–294, 2023.

[26] R. Gusain, K. Gupta, P. Joshi, and O. P. Khatri, "Adsorptive removal and photocatalytic degradation of organic pollutants using metal oxides and their composites: a comprehensive review," *Advances in Colloid and Interface Science*, vol. 272, 2019.

[27] B. Zhang, B. K. Biswal, J. Zhang, and R. Balasubramanian, "Hydrothermal treatment of biomass feedstocks for sustainable production of chemicals, fuels, and materials: progress and perspectives," *Chemical Reviews*, vol. 123, no. 11, pp. 7193–7294, 2023.

[28] M. Jafarian, P. Haseli, S. Saxena, and B. Dally, "Emerging technologies for catalytic gasification of petroleum residue derived fuels for sustainable and cleaner fuel production—an overview," *Energy Reports*, vol. 9, pp. 3248–3272, 2023.

[29] S. Nizamuddin, H. A. Baloch, G. J. Griffin et al., "An overview of effect of process parameters on hydrothermal carbonization of biomass," *Renewable and Sustainable Energy Reviews*, vol. 73, pp. 1289–1299, 2017.

[30] N. Zhou, H. Chen, J. Xi et al., "Biochars with excellent Pb (II) adsorption property produced from fresh and dehydrated banana peels via hydrothermal carbonization," *Bioresource Technology*, vol. 232, pp. 204–210, 2017.

[31] Q. Li, J. Liu, S. Wang et al., "Numerical insights into factors affecting collapse behavior of horizontal wellbore in clayey silt hydrate-bearing sediments and the accompanying control strategy," *Ocean Engineering*, vol. 297, 2024.

[32] T. Avcu, O. Üner, and Ü. Geçgel, "Adsorptive removal of diclofenac sodium from aqueous solution onto sycamore ball activated carbon–isotherms, kinetics, and thermodynamic study," *Surfaces and Interfaces*, vol. 24, 2021.

[33] C. Silveira, Q. L. Shimabuku-Biadola, M. F. Silva, M. F. Vieira, and R. Bergamasco, "Development of an activated carbon impregnation process with iron oxide nanoparticles by green synthesis for diclofenac adsorption," *Environmental Science and Pollution Research*, vol. 27, no. 6, pp. 6088–6102, 2020.

[34] M. M. A. Daouda, A. V. O. Akowanou, S. E. R. Mahunon, C. K. Adjinda, M. P. Aina, and P. Drogui, "Optimal removal of diclofenac and amoxicillin by activated carbon prepared from coconut shell through response surface methodology," *South African Journal of Chemical Engineering*, vol. 38, no. 1, pp. 78–89, 2021.

[35] F. Güzel and F. Koyuncu, "Adsorptive removal of diclofenac sodium from aqueous solution via industrial processed citrus solid waste–based activated carbon: optimization, kinetics, equilibrium, thermodynamic, and reusability analyses," *Biomass Conversion and Biorefinery*, vol. 13, no. 3, pp. 2401–2412, 2023.

[36] I. Langmuir, "The adsorption of gases on plane surfaces of glass, mica and platinum," *Journal of the American Chemical Society*, vol. 40, no. 9, pp. 1361–1403, 1918.

[37] H. M. F. Freundlich, "Over the adsorption in solution," *Journal of Physical Chemistry*, vol. 57, no. 385471, pp. 1100–1107, 1906.

[38] R. D. Johnson and F. H. Arnold, "The Temkin isotherm describes heterogeneous protein adsorption," *Biochimica et Biophysica Acta (BBA)-Protein Structure and Molecular Enzymology*, vol. 1247, no. 2, pp. 293–297, 1995.

[39] S. K. Lagergren, "About the theory of so-called adsorption of soluble substances," *Kungliga Svenska Vetenskapsakademiens, Handlingar*, vol. 24, pp. 1–39, 1898.

[40] Y. S. Ho and G. McKay, "Pseudo-second order model for sorption processes," *Process Biochemistry*, vol. 34, no. 5, pp. 451–465, 1999.

[41] P. S. Kumar, S. Ramalingam, V. Sathyaselvabala, S. D. Kirupha, A. Murugesan, and S. Sivanesan, "Removal of cadmium (II) from aqueous solution by agricultural waste cashew nut shell," *Korean Journal of Chemical Engineering*, vol. 29, no. 6, pp. 756–768, 2012.

[42] Y. Zhang, X. Kang, J. Tan, and R. L. Frost, "Influence of calcination and acidification on structural characterization of Anyang anthracites," *Energy and Fuels*, vol. 27, no. 11, pp. 7191–7197, 2013.

[43] S. U. Awan, S. K. Hasanain, J. Rashid et al., "Structural, optical, electronic, and magnetic properties of multiphase ZnO/Zn (OH) 2/ZnO2 nanocomposites and hexagonal prism-shaped ZnO nanoparticles synthesized by pulse laser ablation in Heptanes," *Materials Chemistry and Physics*, vol. 211, pp. 510–521, 2018.

[44] H. V. Bao, N. M. Dat, N. T. H. Giang et al., "Behavior of ZnO-doped TiO2/rGO nanocomposite for water treatment enhancement," *Surfaces and Interfaces*, vol. 23, 2021.

[45] M. Muttakin, S. Mitra, K. Thu, K. Ito, and B. B. Saha, "Theoretical framework to evaluate minimum desorption temperature for IUPAC classified adsorption isotherms," *International Journal of Heat and Mass Transfer*, vol. 122, pp. 795–805, 2018.

[46] D. Naghipour, L. Hoseinzadeh, K. Taghavi, and J. Jaafari, "Characterization, kinetic, thermodynamic and isotherm data for diclofenac removal from aqueous solution by activated carbon derived from pine tree," *Data in Brief*, vol. 18, pp. 1082–1087, 2018.

[47] E. A. Stepanidenko, I. D. Skurlov, P. D. Khavlyuk et al., "Carbon dots with an emission in the near infrared produced from organic dyes in porous silica microsphere templates," *Nanomaterials*, vol. 12, no. 3, p. 543, 2022.

[48] M. Sevilla and A. B. Fuertes, "Chemical and structural properties of carbonaceous products obtained by hydrothermal carbonization of saccharides," *Chemistry--A European Journal*, vol. 15, no. 16, pp. 4195–4203, 2009.

[49] J. Peng, X. Kang, S. Zhao et al., "Growth mechanism of glucose-based hydrochar under the effects of acid and temperature regulation," *Journal of Colloid and Interface Science*, vol. 630, pp. 654–665, 2023.

[50] Y. Li, H. Lu, Y. Wang, Y. Zhao, and X. Li, "Efficient removal of methyl blue from aqueous solution by using poly (4-vinylpyridine)–graphene oxide–Fe3O4 magnetic nanocomposites," *Journal of Materials Science*, vol. 54, no. 10, pp. 7603–7616, 2019.

[51] R. Zandipak and S. Sobhanardakani, "Novel mesoporous Fe 3 O 4/SiO 2/CTAB–SiO 2 as an effective adsorbent for the removal of amoxicillin and tetracycline from water," *Clean Technologies and Environmental Policy*, vol. 20, no. 4, pp. 871–885, 2018.

[52] M. Ghoochian, H. A. Panahi, S. Sobhanardakani, L. Taghavi, and A. H. Hassani, "Synthesis and application of Fe3O4/SiO2/thermosensitive/PAMAM-CS nanoparticles as a novel adsorbent for removal of tamoxifen from water samples," *Microchemical Journal*, vol. 145, pp. 1231–1240, 2019.

[53] M. Ghafoori, M. Cheraghi, M. K. Sadr, B. Lorestani, and S. Sobhanardakani, "Magnetite graphene oxide modified with β-cyclodextrin as an effective adsorbent for the removal of methotrexate and doxorubicin hydrochloride from water," *Environmental Science and Pollution Research*, vol. 29, no. 23, pp. 35012–35024, 2022.

[54] H. Gupta, "Removal of phenanthrene from water using activated carbon developed from orange rind," *International Journal of Scientific Research in Environmental Sciences*, vol. 3, no. 7, pp. 248–255, 2015.

[55] R. Lafi, I. Montasser, and A. Hafiane, "Adsorption of Congo red dye from aqueous solutions by prepared activated carbon with oxygen-containing functional groups and its regeneration," *Adsorption Science and Technology*, vol. 37, no. 1-2, pp. 160–181, 2019.

[56] N. A. Fathy and S. El-Shafey, "Carbon-based nanohybrid fabricated in-situ and boosted the adsorption of anionic reactive yellow dye," *International journal of Environmental Science and Technology*, vol. 20, no. 1, pp. 293–306, 2023.

[57] M. Antunes, V. I. Esteves, R. Guégan, J. S. Crespo, A. N. Fernandes, and M. Giovanela, "Removal of diclofenac sodium from aqueous solution by Isabel grape bagasse," *Chemical Engineering Journal*, vol. 192, pp. 114–121, 2012.

[58] G. S. Maia, J. R. de Andrade, M. G. da Silva, and M. G. Vieira, "Adsorption of diclofenac sodium onto commercial organoclay: kinetic, equilibrium and thermodynamic study," *Powder Technology*, vol. 345, pp. 140–150, 2019.

[59] P. V. Viotti, W. M. Moreira, O. A. A. d. Santos, R. Bergamasco, A. M. S. Vieira, and M. F. Vieira, "Diclofenac removal from water by adsorption on Moringa oleifera pods and activated carbon: mechanism, kinetic and equilibrium study," *Journal of Cleaner Production*, vol. 219, pp. 809–817, 2019.

[60] B. A. Abdel Majeed, R. J. Muhseen, and N. J. Jassim, "Adsorption of diclofenac sodium and ibuprofen by bentonite polyureaformaldehyde thermodynamics and kinetics study," *Iraqi Journal of Chemical and Petroleum Engineering*, vol. 19, no. 1, pp. 29–43, 2018.

[61] I. M. Jauris, C. F. Matos, C. Saucier et al., "Adsorption of sodium diclofenac on graphene: a combined experimental and theoretical study," *Physical Chemistry Chemical Physics*, vol. 18, no. 3, pp. 1526–1536, 2016.

[62] X. X. Liang, A. M. Omer, Z. H. Hu, Y. G. Wang, D. Yu, and X. K. Ouyang, "Efficient adsorption of diclofenac sodium from aqueous solutions using magnetic amine-functionalized chitosan," *Chemosphere*, vol. 217, pp. 270–278, 2019.